Robotica (2025), 1–19
doi:10.1017/S0263574725102464

CAMBRIDGE UNIVERSITY PRESS

RESEARCH ARTICLE

Analysis and development of the modular elements of a tendon-actuated glove for hand rehabilitation

Mihai Dragusanu, Alessio Piroli and Monica Malvezzi

Department of Information Engineering and Mathematics, University of Siena, Siena, Italy
Corresponding author: Monica Malvezzi; Email: monica.malvezzi@unisi.it

Received: 15 March 2025; **Revised:** 1 July 2025; **Accepted:** 16 August 2025

Keywords: exoskeletons; robotic rehabilitation; wearable robotics

Abstract

Robotic rehabilitation requires personalized, versatile, and efficient devices to accommodate the diverse needs of patients recovering from motor impairments. In this paper, we focus on hand rehabilitation and analyse a tendon-driven, modular, and adaptable robotic glove actuated by twisted string actuators (TSAs). The proposed solution exploits flexibility in design, allowing customization based on individual patient needs while ensuring effective assistance in hand movements.

Specifically, in this paper we investigate the kinematic relationships between tendon-driven actuators and hand motion. We provide a detailed implementation of multiple functional modules within the glove, designed to accommodate various rehabilitation exercises and adapt to different degrees of motor impairment. In addition, we present experimental tests involving a user to evaluate the system's performance, usability, and effectiveness in facilitating hand movement. The results provide insights into the potential of TSA-driven robotic gloves for enhancing rehabilitation outcomes through a combination of precise actuation and adaptability to user's needs.

1. Introduction

Integrating robotics in rehabilitation has disruptive potential in patient care, offering personalized, efficient, and effective treatment modalities across various conditions [1]. By harnessing the power of these technologies, healthcare providers can enhance the quality and accessibility of rehabilitation services, improving patient outcomes and quality of life. Telerehabilitation stands at the forefront of digital healthcare innovation, forecasted to leap with a compound annual growth rate (CAGR) of 15.3% from 2023 to 2030.[1] Robotic technologies are progressing fast, delivering new and powerful technologies in different fields, including rehabilitation, that create new opportunities for people and are potentially able to transform the rehabilitation process shortly, as well as new challenges and responsibilities to be elucidated and contained [2].

Concerning hand and upper limb rehabilitation devices, we recently proposed an impairment-based roadmap for device classification, selection, and design [3]. In such a work, devices were classified into three main classes, namely rigid, soft, and hybrid. Rigid exoskeletons [4, 5] are usually employed when higher forces and precise motion tracking are required but are less adaptable and wearable. On the opposite side, soft actuated gloves, employing soft materials and tendon-based [6] or pneumatic actuation [7], are more comfortable for the user, even if can exert more limited forces.

Twisted string actuators (TSA) have been recently employed in exoskeleton and actuated suits for the arm [8], the elbow [9], the knee [10], the hip [11], and the hand [12]. TSAs are substantially a rotary-to-linear transmission system based on the principle that twisting a series of strings shortens their length [13, 14]. TSAs are constituted by a motor, a set of strings, and a load (to keep the strings in tension). TSAs

[1] https://www.grandviewresearch.com/industry-analysis/telerehabilitation-market-report

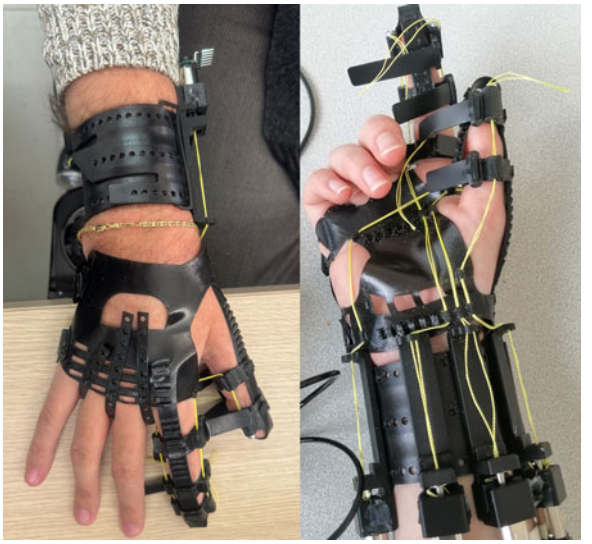

Figure 1. *The glove with the thumb and index modules worn by two users.*

have very low transmission ratios, and therefore very high force transmission ratios and can be realized using small and light motors. These characteristics made them convenient in different applications, for instance, soft robots or exoskeletons. In this last application, in particular, TSA allows light and wearable solutions.

A tendon-actuated glove driven by TSA has been introduced in ref. [15]. Tendons were arranged to actuate both the adduction/abduction and the flexion motion of the thumb and the fingers, and the extension motion was passively obtained with an elastic element storing potential energy during the actuated flexion motion and releasing it in the extension motion. In the paper, we demonstrated the feasibility of a complete hand system with 10 actuators and presented some preliminary evaluations in which a potential user was employed. The proposed system was modular and potentially extensible to different types of finger actuation. Figure 1 shows two users wearing the glove with the thumb and index finger actuated.

In ref. [3], the PICO (Problem / Population Intervention Comparison Outcome) approach, broadly used in evidence-based medicine (EBM) to structure clinical questions, was proposed for designing and classifying robotic rehabilitation devices, focusing in particular on hand exoskeleton. According to such an approach, in which the P-term was presented with an impairment-oriented perspective, the device presented in ref. [15] is suitable for all pathologies and injuries that lead to range of motion (ROM) limitation, strength reduction, and coordination disorders with limited or no spasticity [16]. The device can be potentially applied, for example, to patients suffering peripheral nerve injuries or musculoskeletal tendon rupture, or in pathologies characterized by progressive muscle weakness, like limb-girdle muscular dystrophy (LGMD). In assistive applications, the design requirements are even more demanding in terms of lightness, adaptability to users' specific needs, versatility, and ease of use [17] with respect to rehabilitation.

Notwithstanding the potentially interesting characteristics, the work presented in ref. [15] did not provide general analytical and numerical models for system evaluation. This work further investigates the mechanical behavior od the actuated glove by analyzing the roles of tendons' anchor points and routing paths on glove capabilities. In particular, we propose a parametric biomechanical hand and wrist model integrated with a general and customizable tendon system in which we can simulate both different anthropometric hand characteristics and different tendon arrangements. We use the proposed model to evaluate four different solutions for the index finger and the wrist: the first one (Figure 2a) employs two pairs of tendons, twisted by two different motors, and the second one is actuated by two single tendons

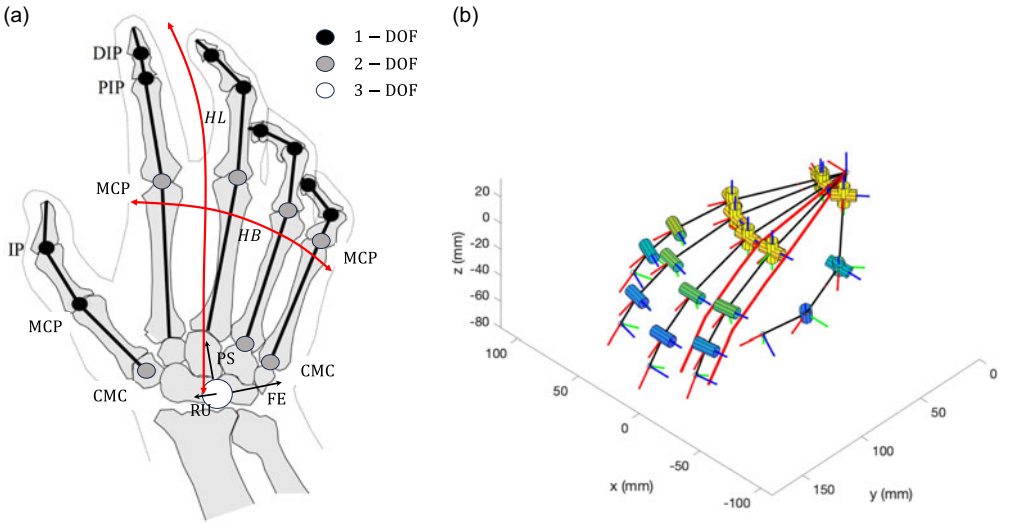

Figure 2. *Schemes of the 28-DOF hand model. (a) Hand/wrist 28-DOF scheme: the wrist is represented as a 3-DOF spherical joint, CMC joints for the thumb, ring, and little finger, and PMC joints are modeled as 2-DOF universal joints, IP joints are modeled as 1-DOF revolute joints. (b) Hand/wrist model realized in Syngrasp, with two tendons (in red) for index finger actuation.*

that are coupled close to the wrist and are twisted by the same motor. The third analyzed configuration actuates index finger flexion/extension movement with two independent tendons, while the fourth investigates the possibility of actuating the three DOFs of the wrist. Through this model, we exploit the possibility of further simplifying the glove structure by actuating each finger with a single tendon and realizing different types of motions (e.g., active flexion/extension). Finally, two different prototypes for finger actuation based on tendon arrangements analyzed previously are presented and evaluated by a user. The first one is based on two TSAs and allows flexion/extension and adduction/abduction motions, while the second one is based on two tendons actuated by the same TSA and allows the flexion–extension motion only.

The paper is organized as follows. Section 2 presents the hand kinematic model and the procedures for glove kinematics and static analysis. Section 3 presents four examples of hand and wrist actuation and their kinematic analysis. Section 4 introduces two actuated glove prototypes, and in Section 5, a set of preliminary experiments is presented. Section 6 discusses numerical and preliminary experimental results, and Section 7 summarizes the work and introduces its future developments.

2. Methodology

2.1. Definitions and assumptions

A preliminary simplified model of glove kinematics has been introduced in ref. [15], where a specific implementation was simulated. In this paper, we systematically extend the procedure, so that different actuation systems can be easily defined and simulated. Syngrasp functions, developed to model and analyze grasp and manipulation tasks with human and robotic hands, have been integrated to include the possibility of simulating finger actuation using tendons.

The kinematics analysis is based on the positions of anchor points defining tendon's routing. We define a tendon anchor point $A_{j,f,l,i}$ by specifying:

- The tendon index j: an integer positive numerical tag for tendon identification, j varies from 1 to n_t, number of tendons;

- The finger index f: a tag for forearm/palm/finger identification, assuming the following values: f-forearm, p-palm, t-thumb, i-index, m-middle, r-ring, and p-little. For the sake of numerical implementation, we assigned the integer values to f varying from $f = -1$ for the forearm, $f = 0$ for the palm, $f = 1$ to 5 for the hand fingers, from the thumb to the little finger;
- The link index l, an integer numerical tag for link identification, within the finger, varying from 0 to the number of links of the specific finger $n_{l,f}$ (the palm and the forearm have one link only, indicated with 0);
- An integer positive index i for indicating the order of the anchor in the tendon routing, starting from 1, the point where the tendon end is fixed on the finger or the palm, and increasing toward the actuator, up to $n_{a,j}$ (i.e., $n_{a,j}$ represents the number of anchor points of tendon j);
- The coordinates $\mathbf{r}_a^{f,l} = [x_a^{f,l}, y_a^{f,l}, z_a^{f,l}]^{\mathrm{T}}$ of the anchor point, expressed in the local link reference frame $\mathcal{S}_{f,l}$, on the l-th link of the f-th finger, where the anchor point is connected, we assume that such points are assigned and that they do not vary during hand motion, i.e., we neglect the anchor point sliding over user's skin and hand deformation.

2.2. Hand biomechanics

A 28-DOF model of the hand/wrist biomechanics has been developed purposely for this work in Syngrasp Toolbox [18, 19], and its scheme is reported in Figure 3. The model is composed of a 25-DOF model of the hand and a 3-DOF model of the wrist. The hand model was developed based on the hypotheses proposed in ref. [20]. We chose this model, among the ones available in the literature, due to its completeness in hand motion representation and easy adaptability to different hand sizes and characteristics [21], since the dimensions of all the links can be varied by changing two parameters only, namely hand length, *HL*, and hand width, *HB*.

The thumb is modeled as a 5-DOF system: 2-DOF (adduction/abduction and extension/flexion) for the carpometacarpal (CMC) joint, 2-DOF (extension/flexion, adduction/abduction)for the metacarpophalangeal (MCP) joint, and 1-DOF (extension/flexion) for the interphalangeal (IP) joint. The index and the middle fingers are modeled as two 4-DOF systems: 2-DOF (extension/flexion, adduction/abduction) for the MCP joints and 1-DOF (extension/flexion) for the proximal-interphalangeal (PIP) and distal-interphalangeal (DIP) joints. The ring and the little fingers are modeled as two 6-DOF systems: two 2-DOF for the CMC joints, to provide the palm arc motion, 2-DOF for the MPC joints, and 1-DOF for the PIP and DIP joints. The wrist motion can be represented as a 3-DOFs spherical joint, including flexion/extension (FE), radial/ulnar (RU) deviation, and pronation/supination (PS).

The base reference frame for hand configuration has the origin in the wrist center, O_0, axes x_0 and y_0 are on the coronal plane, and y_0 is aligned with the sagittal plane. A second reference frame relative to the palm is defined, its origin coincides with O_0 and the axes x_p, y_p z_p coincide with the base when the wrist is in the reference configuration. Five auxiliary reference frames are defined to describe fingers' kinematics; the origins $O_{0,t}$, $O_{0,r}$, and $O_{0,l}$, relative to the thumb, ring, and little fingers, are in the corresponding CMC joint centers, while the origins O_i and O_m, relative to the index and middle fingers are in the corresponding MCP joint centers. The homogeneous transform matrix $\mathbf{T}_{O,t}^{p}$ relating the thumb auxiliary frame with the palm frame is defined as

$$\mathbf{T}_{O,t}^{p} = \begin{bmatrix} \cos\gamma_t & -\sin\gamma_t & 0 & -l_{0,t}\sin\gamma_t \\ \sin\gamma_t & \cos\gamma_t & 0 & 0 \\ 0 & 0 & 1 & l_{0,t}\cos\gamma_t \\ 0 & 0 & 0 & 1 \end{bmatrix} \tag{1}$$

with

$$l_{0,t} = 0.118HL \tag{2}$$

Table I. *Hand joints: description and range of motion (ROM).*

Joint variable	Description	q_{min} (degrees)	q_{max} (degrees)
q_1	thumb, CMC, add./abd.	0	60
q_2	thumb, CMC, flex./ext.	25	35
q_3	thumb, MCP, flex./ext.	−55	10
q_4	thumb, MCP, add./abd.	0	60
q_5	thumb, IP, flex/ext	−15	0
q_6	index, MPC, add./abd.	−13	42
q_7	index, MPC, flex./ext.	0	80
q_8	index, PIP, flex./ext.	0	100
q_9	index, DIP, flex./ext.	−10	90
q_{10}	middle, MPC, add./abd.	−8	35
q_{11}	middle, MPC, flex./ext.	0	80
q_{12}	middle, PIP, flex./ext.	0	100
q_{13}	middle, DIP, flex./ext.	−10	90
q_{14}	ring, CMC, add./abd.	0	5
q_{15}	ring, CMC, flex./ext.	0	10
q_{16}	ring, MPC, add./abd.	−14	20
q_{17}	ring, MPC, flex./ext.	0	80
q_{18}	ring, PIP, flex./ext.	0	100
q_{19}	ring, DIP, flex./ext.	−20	90
q_{20}	little, CMC, add./abd.	0	5
q_{21}	little, CMC, flex./ext.	0	10
q_{22}	little, MPC, add./abd.	−19	33
q_{23}	little, MPC, flex./ext.	0	80
q_{24}	little, PIP, flex./ext.	0	100
q_{25}	little, DIP, flex./ext.	−30	90
q_{26}	wrist flex./ext.	−90	90
q_{27}	wrist radio/ulnar dev.	−35	35
q_{28}	wrist pron./sup.	−30	90

and $\gamma_t = 40°$. Homogeneous transformation matrices for the other fingers can be similarly defined, with the following parameters for the displacements $l_{0,\circ}$ and angles $\gamma_\circ$, with $\circ = [i, m, r, l]$:

$$\begin{aligned} l_{0,i} &= \sqrt{0.374HL^2 + 0.126HB^2} \\ l_{0,m} &= 0.373HL \\ l_{0,r} &= 0.09HB \\ l_{0,l} &= 0.1HB \end{aligned} \tag{3}$$

$$\begin{aligned} \gamma_i &= 7° \\ \gamma_m &= 13° \\ \gamma_r &= 14° \\ \gamma_l &= 25° \end{aligned} \tag{4}$$

Hand kinematics can be modeled using Denavit–Hartenberg convention and parameters. Hand configuration is therefore represented by the vector $\mathbf{q} \in \Re^{28}$, containing joint angles. Parameters $q_1, \cdots, q_5$ are relative to the thumb, $q_6, \cdots, q_9$ to the index, $q_{10}, \cdots, q_{13}$ to the middle, $q_{14}, \cdots, q_{19}$ to the ring, and $q_{20}, \cdots, q_{25}$ to the little finger, q_{26} represents wrist pronation/supination movement, q_{27} represents wrist radial/ulnar deviation, and q_{28} represent wrist flexion/extension. Table I summarizes hand joint index, description, and ROM.

Table II. *Thumb: Denavit–Hartenberg parameters.*

Joint n.	Joint id	a_i	α_i (rad)	d_i	θ_i (rad)
1	1,1	0	$-\pi/2$	0	$\pi/2+q_1$
2	1,2	l_{1t}	$\pi/2$	0	q_2
3	1,3	0	$-\pi/2$	0	q_3
4	1,4	l_{2t}	$\pi/2$	0	q_4
5	1,5	l_{3t}	$-\pi/2$	0	q_5

Table III. *Index and middle: Denavit–Hartenberg parameters.*

Joint n.	f,l	a_i	α_i (rad)	d_i	θ_i (rad)	Joint n.	f,l	a_i	α_i (rad)	d_i	θ_i (rad)
6	2,1	0	$-\pi/2$	0	$\pi/2+q_6$	10	3,1	0	$-\pi/2$	0	$\pi/2+q_{10}$
7	2,2	l_{1i}	0	0	q_7	11	3,2	l_{1m}	0	0	q_{11}
8	2,3	l_{2i}	0	0	q_8	12	3,3	l_{2m}	0	0	q_{12}
9	2,4	l_{3i}	0	0	q_9	13	3,4	l_{3m}	0	0	q_{13}

Table IV. *Ring and Little: Denavit Hartenberg parameters.*

Joint n.	f,l	a_i	α_i (rad)	d_i	θ_i (rad)	Joint n.	f,l	a_i	α_i (rad)	d_i	θ_i (rad)
14	4,1	0	$-\pi/2$	0	$\pi/2+q_{14}$	20	5,1	0	$-\pi/2$	0	$\pi/2+q_{20}$
15	4,2	l_{1r}	$\pi/2$	0	q_{15}	21	5,2	l_{1l}	$\pi/2$	0	q_{21}
16	4,3	0	$-\pi/2$	0	q_{16}	22	5,3	0	$-\pi/2$	0	q_{22}
17	4,4	l_{2r}	0	0	q_{17}	23	5,4	l_{2l}	0	0	q_{23}
18	4,5	l_{3r}	0	0	q_{18}	24	5,5	l_{3l}	0	0	q_{24}
19	4,6	l_{4r}	0	0	q_{19}	25	5,6	l_{4l}	0	0	q_{25}

Table V. *Wrist: Denavit Hartenberg parameters.*

Joint n.	f,l	a_i	α_i (rad)	d_i	θ_i (rad)
26	0,1	0	$-\pi/2$	0	q_{26}
27	0,2	0	$\pi/2$	0	q_{27}
28	0,3	0	0	0	q_{28}

The model is parametric and easy to adapt to different hand sizes: the dimensions of all the links can be varied by changing two parameters only, namely hand length, *HL*, and hand width *HB*. Tables II, III, IV, and V summarize Denavit–Hartenberg parameters for the thumb, index/middle, ring/little, and wrist, respectively. Link lengths are evaluated as a function of *HL* and *HB* as follows:

$$\begin{cases} l_{1t} = 0.251HL \\ l_{2t} = 0.196HL \\ l_{3t} = 0.158HL \end{cases} \tag{5}$$

$$\begin{cases} l_{1i} = 0.265HL \\ l_{2i} = 0.143HL \\ l_{3i} = 0.097HL \end{cases} \tag{6}$$

$$\begin{cases} l_{1r} = \sqrt{0.336HL^2 + 0.077HB^2} \\ l_{2r} = 0.259HL \\ l_{3r} = 0.165HL \\ l_{4r} = 0.107HL \end{cases} \tag{7}$$

$$\begin{cases} l_{1l} = \sqrt{0.295HL^2 + 0.179HB^2} \\ l_{2l} = 0.206HL \\ l_{3l} = 0.117HL \\ l_{4l} = 0.093HL \end{cases} \tag{8}$$

2.3. Inverse kinematics

In this context, we indicate with inverse kinematics the algorithm allowing to find the actuator configuration, i.e., the set of tendon strokes $\mathbf{s} = [s_1, \cdots, s_{n_a}]$, corresponding to a given hand configuration $\mathbf{q}$, i.e.,

$$\mathbf{s} = \mathbf{f}_{ik}(\mathbf{q}). \tag{9}$$

Standard forward kinematics relationships [22] for the fingers already present in Syngrasp tool and adapted for this purpose allow the evaluation of anchor points' position during hand and wrist motion. In particular, for a given configuration represented by joints $\mathbf{q}$, the coordinates of the generic anchor point in the base (forearm) reference frame can be defined as

$$\tilde{\mathbf{r}}_{i,j} = \mathbf{T}^0_{-1}\mathbf{T}^{f,l}_0\tilde{\mathbf{r}}^{f,l}_{i,j}, \tag{10}$$

where $\mathbf{T}^{f,l}_0 \in \Re^{4\times4}$ is the homogeneous transformation matrix between the base reference frame and the link reference frame, depending on the hand's configuration, that can be evaluated using Denavit–Hartenberg parameters previously introduced, and $\tilde{\mathbf{r}}_a$ and $\tilde{\mathbf{r}}^{f,l}_i$ are the homogeneous representations of $\mathbf{r}_{i,j}$ and $\mathbf{r}^{f,l}_{i,j}$, respectively (i.e., $\tilde{\mathbf{r}}_a = [\mathbf{r}^{\mathrm{T}}_a, 1]^{\mathrm{T}}$).

Specifically, $\mathbf{T}^{f,l}_0$ can be evaluated as follows:

$$\mathbf{T}^{f,l}_0 = \prod_{f,k=1}^{l} \mathbf{T}^{f,k}_{k-1} \tag{11}$$

where $\mathbf{T}^{f,k}_{k-1}$ is evaluated according to Denavit–Hartenberg parameters defined in Tables II, III, IV, and V, as

$$\mathbf{T}^{f,k}_{k-1} = \begin{bmatrix} \cos\theta_{f,k} & -\sin\theta_{f,k}\cos\alpha_{f,k} & \sin\theta_{f,k}\sin\alpha_{f,k} & a_{f,k}\cos\theta_{f,k} \\ \sin\theta_{f,k} & \cos\theta_{f,k}\cos\alpha_{f,k} & -\cos\theta_{f,k}\sin\alpha_{f,k} & a_{f,k}\sin\theta_{f,k} \\ 0 & \sin\alpha_{f,k} & \cos\alpha_{f,k} & d_{f,k} \\ 0 & 0 & 0 & 1 \end{bmatrix}. \tag{12}$$

$\mathbf{T}^0_{-1}$ is the homogeneous transformation matrix between the forearm and the palm. Assuming both the forearm and palm reference frames origins in the wrist rotation center, such a matrix is defined as

$$\mathbf{T}^0_{-1} = \begin{bmatrix} \cos q_{28} & -\sin q_{28} & 0 & 0 \\ \sin q_{28} & \cos q_{28} & 0 & 0 \\ 0 & 0 & 1 & 0 \\ 0 & 0 & 0 & 1 \end{bmatrix} \begin{bmatrix} \cos q_{26} & 0 & \sin q_{26} & 0 \\ 0 & 1 & 0 & 0 \\ -\sin q_{26} & 0 & \cos q_{26} & 0 \\ 0 & 0 & 0 & 1 \end{bmatrix} \begin{bmatrix} 1 & 0 & 0 & 0 \\ 0 & \cos q_{27} & \sin q_{27} & 0 \\ 0 & -\sin q_{27} & \cos q_{27} & 0 \\ 0 & 0 & 0 & 1 \end{bmatrix}. \tag{13}$$

Given the positions of the anchor points of the j-th tendon, defined in the base reference frame, the corresponding tendon length l_j can be evaluated as

$$l_j = \sum_{i=2}^{n_{a,j}} ||\mathbf{r}_{i,j} - \mathbf{r}_{i-1,j}||, \tag{14}$$

Tendon lengths are collected in the vector $\mathbf{l} = [l_1, \cdots, l_{n_t}]^{\mathrm{T}} \in \Re^{n_t}$. The displacement that has to be applied by the actuator is then evaluated as

$$s_j = l_{j,0} - l_j, \tag{15}$$

Algorithm 1. Inverse kinematics algorithm

function $\mathbf{s} = \mathbf{f}_{ik}(\mathbf{q})$
  $\mathbf{T}^0_{-1} \leftarrow \mathbf{T}^0_{-1}(q_{26}, q_{27}, q_{28})$ ▷ Eq. (13)
  for $j = 1{:}n_t$ **do**
    $l_j = 0$
    for $i = 1{:}n_{a,j}$ **do**
      $\mathbf{T}^l_0 \leftarrow \mathbf{I}_{4\times4}$
      for $k = 1{:}l$ **do**
        $\mathbf{T}^{f,k}_{k-1} \leftarrow \mathbf{T}^{f,k}_{k-1}(\mathbf{q})$ ▷ Eq. (12)
        $\mathbf{T}^l_0 \leftarrow \mathbf{T}^l_0 \mathbf{T}^{f,k}_{k-1}$ ▷ Eq. (11)
      end for
      $\tilde{\mathbf{r}}_{i,j} \leftarrow \mathbf{T}^0_{-1} \mathbf{T}^{f,l}_0 \tilde{\mathbf{r}}^{f,l}_{i,j}$ ▷ Eq. (10)
      if $i > 1$ **then**
        $l_j = l_j + \|\mathbf{r}_{i,j} - \mathbf{r}_{i-1,j}\|$ ▷ Eq. (14)
      end if
    end for
    $s_j = l_{j,0} - l_j$ ▷ Eq. (15)
  end for
end function

where $l_{j,0}$ is tendon length in hand reference configuration. The inverse kinematics function is summarized in Algorithm 1. Let us further collect the positions of all the anchor points in a vector $\mathbf{r}_a = [\mathbf{r}^{\mathrm{T}}_{1,1}, \cdots, \mathbf{r}^{\mathrm{T}}_{n_t,n_{a,nt}}]^{\mathrm{T}} \in \Re^{3n_a}$, where $n_a = \sum_{j=1}^{n_t} n_{a,j}$.

2.4. Inverse differential kinematics

Standard differential kinematics relationships [22] can be straightforwardly used to define the anchor point Jacobian matrix $\mathbf{J}_a \in \Re^{3na \times n_q}$ relating anchor point velocities

$$\mathbf{v}_a = [\mathbf{v}^{\mathrm{T}}_{a,1,1}, \cdots, \mathbf{v}^{\mathrm{T}}_{a,n_t,n_{a,nt}}]^{\mathrm{T}} \in \Re^{3na},$$

where $\mathbf{v}_{a,i} = \frac{d\mathbf{r}_i}{dt}$ is the velocity of the i-th anchor point, to joint angular velocities $\dot{\mathbf{q}}$, namely:

$$\mathbf{v}_a = \mathbf{J}_a \dot{\mathbf{q}}. \tag{16}$$

Let us consider a generic pair of adjacent anchor points $A_{i,j}, A_{i+1,j}$ on the generic tendon, j. The previously introduced equation allows us to evaluate their velocities $\mathbf{v}_{a,i,j}$ and $\mathbf{v}_{a,i+1,j}$ for a given hand configuration and velocity. The time derivative of tendon length between such points is defined by

$$\dot{l}_{(i,i+1),j} = (\mathbf{v}_{a,i,j} - \mathbf{v}_{a,i+1,j}) \cdot \mathbf{u}_{i-i+1,j}, \tag{17}$$

where $\mathbf{u}_{i-i+1,j}$ is the unit vector identifying the direction between $A_{i,j}$ and $A_{i+1,j}$ points, i.e.,

$$\mathbf{u}_{i-i+1,j} = \frac{\mathbf{r}_{i,j} - \mathbf{r}_{i,j}}{||\mathbf{r}_{i,j} - \mathbf{r}_{i,j}||}. \tag{18}$$

The overall tendon velocity is defined as

$$\dot{l}_j = \sum_{i_1}^{n_{a,j}-1} \dot{l}_{(i,i+1),j} = \sum_{i_1}^{n_{a,j}-1} \mathbf{u}^{\mathrm{T}}_{i-i+1,j}(\mathbf{v}_{a,i,j} - \mathbf{v}_{a,i+1,j}), \tag{19}$$

that can be rewritten as

$$\dot{l}_j = \mathbf{J}_{t,j} \mathbf{v}_{a,j}, \tag{20}$$

where

$$\mathbf{J}_{t,j} = [\mathbf{u}_{1,j}, -\mathbf{u}_{1,j} + \mathbf{u}_{2,j}, \cdots, -\mathbf{u}_{n_{a,j},j}]. \tag{21}$$

By analyzing anchor point velocities, it is possible to define a relationship between tendon velocities $\dot{\mathbf{l}} = [\dot{l}_1, \cdots, \dot{l}_{n_a}]^{\mathrm{T}}$ and anchor point velocities $\mathbf{v}_a$, namely,

$$\dot{\mathbf{l}} = \mathbf{J}_t \mathbf{v}_a. \tag{22}$$

Therefore, a relationship between tendon velocities and hand joint angular velocity can be established as $\dot{\mathbf{l}} = \mathbf{J}\dot{\mathbf{q}}$, where $\mathbf{J} = \mathbf{J}_t\mathbf{J}_a \in \Re^{n_t \times n_q}$ is the exoskeleton Jacobian.

2.5. Statics

By applying the principle of virtual work, and assuming that the constraints imposed by anchor points are frictionless and neglecting the friction along the tendon path, it is possible to define a relationship between hand/wrist joint torques $\boldsymbol{\tau} \in \Re^{n_q}$ and tendon forces $\mathbf{f} \in \Re^{n_t}$, i.e.,

$$\boldsymbol{\tau} = \mathbf{J}^{\mathrm{T}}\mathbf{f}. \tag{23}$$

where $\boldsymbol{\tau} \in \Re^{n_q}$ is the vector of joint torques, while $\mathbf{f} \in \Re^{n_t}$ is a vector containing tendon forces. To implement a force control on the device, such relationship has to be inverted, i.e., a set of tendon forces $\mathbf{f}$ have to be defined to obtain a certain torque $\boldsymbol{\tau}$. The problem cannot be straightforwardly solved for the complete hand/wrist system, due to hand fingers' glove underactuation [15]. However, if we consider subsystems as for instance wrist actuation only, we can assume for the sake of conciseness $n_q = 3$. An example that will be presented in the following section for wrist actuation is actuated by $n_t = 5$ actuators, so for this subproblem, the transpose of the Jacobian matrix $\mathbf{J}^{\mathrm{T}}$ dimensions are 3×5. If the matrix is full-rank, the linear system in Eq. (23) has infinite solutions, that can be represented as

$$\mathbf{f} = (\mathbf{J}^{\mathrm{T}})^{+}\boldsymbol{\tau} + \mathbf{N}_{Jt}\boldsymbol{\xi} \tag{24}$$

where $\mathbf{N}_{Jt}$ is a basis of $\mathbf{J}^{\mathrm{T}}$ nullspace and $\boldsymbol{\xi}$ is an arbitrary vector. Force vectors defined by

$$\mathbf{f}_i = \mathbf{N}_{Jt}\boldsymbol{\xi} \tag{25}$$

represent a set of forces such that $\mathbf{J}^{\mathrm{T}}\mathbf{f}_i = \mathbf{0}$, i.e., the set of tendon forces that do not apply torques to hand and wrist joint. Such forces can be exploited in device control for example to guarantee that tendons are tight during the whole exercise.

In the device proposed in this paper, tendons are actuated by TSA. Therefore, the analysis should be complemented by including the actuator transmission, i.e., the relationship between tendon length variation s_j and motor rotation θ_j. This aspect is important, due to the peculiar nonlinear behavior of this type of actuator, and has been comprehensively investigated in previous studies, e.g. [13, 23].

3. Simulation of hand exercises

The tendons and anchor points $A_{j,f,l,i}$ for four different configurations for index finger and wrist actuation analyzed in the following sections are schematically shown in Figure 2. The positions of the anchor points were defined with heuristic considerations, mainly taking into account the constraints due to the specific characteristics of the hardware components used in the prototype. Specifically, in Figure 2a, the index finger is actuated with two tendons enabling adduction/abduction and flexion motion, in Figure 2b, the two tendons are connected to the same TSA, enabling flexion motion only, in Figure 2c, the index finger is actuated with two tendons enabling extension and flexion motion, in Figure 2d, the wrist is actuated with five tendons enabling flexion/extension, radial/ulnar deviation, and pronation/supination. For each of the above introduced configutations, anchor points' locations expressed in the corresponding (local) reference frame are summarized in Tables VI, VII, VIII, and IX, respectively.

The above-described kinematic models of the hand and the tendons have been implemented in Syngrasp [18, 19], and the execution of a series of rehabilitation exercises has been simulated. The

Table VI. *Index actuation with two tendons, adduction/abduction, and flexion. Anchor points coordinates in the local reference frames.*

Tendon id.	Anchor id.	$x_a^{f,l}$ (mm)	$y_a^{f,l}$ (mm)	$z_a^{f,l}$ (mm)	Note on anchor point position
1					
	$A_{1,2,4,1}$	19	0	0	Finger tip
	$A_{1,2,4,2}$	0	0	−7	Along DIP axis
	$A_{1,2,3,3}$	12	0	−8	Middle of IP
	$A_{1,2,2,4}$	17	0	−8	Middle of PP
	$A_{1,2,2,5}$	0	0	−9	Along MCP axis
	$A_{1,0,0,6}$	52	−7	−22	Palm
	$A_{1,0,0,7}$	29	−7	−20	Palm
	$A_{1,0,0,8}$	0	−7	−15	Wrist
	$A_{1,-1,0,9}$	−23	−10	−10	Forearm
2					
	$A_{2,2,4,1}$	19	0	0	Finger tip
	$A_{2,2,4,2}$	0	0	7	Along DIP axis
	$A_{2,2,3,3}$	12	0	8	Middle of IP
	$A_{2,2,2,4}$	17	0	8	Middle of PP
	$A_{2,0,0,5}$	52	−7	−10	Palm
	$A_{2,0,0,6}$	29	−7	−8	Palm
	$A_{2,0,0,7}$	0	−7	−7	Wrist
	$A_{2,-1,0,8}$	−23	−10	−2	Forearm

Table VII. *Index actuation with two tendons connected to the same TSA. Anchor points coordinates in the local reference frames.* $A_{1,2,4,1}, \cdots A_{1,0,0,8}$ *and* $A_{2,2,4,1}, \cdots A_{2,0,0,7}$ *are the same as in Table VI.*

Tendon id.	Anchor id.	$x_a^{f,l}$ (mm)	$y_a^{f,l}$ (mm)	$z_a^{f,l}$ (mm)	Note on anchor point position
1					
	...	...	...	...	...
	$A_{1,-1,0,9}$	−23	−10	−8	Forearm
2					
	...	...	...	...	...
	$A_{2,-1,0,8}$	−23	−10	−8	Forearm

objective of the simulation was to define the stroke of the tendons necessary to realize the motion. This information is needed in the following part of device development, to dimension the TSA characteristics. The four different tendon arrangements schematized in Figure 2 have been simulated. In particular, to test the versatility of the proposed approach, we have considered three different arrangements with two tendons for the index finger (Figure 2a, b, and c) and a five-tendon configuration for the wrist (Figure 2d). In all the simulations, the movement has been executed in 5s. Simulation results are graphically represented in Figure 4.

The first simulation refers to tendon configuration in Figure 2a, in which the index is actuated with two independent tendons. The simulated movement is finger flexion starting from the reference configuration, coupled with MCP joint adduction. The final value for q_7 joint has been set to 60°, while q_6, q_8, and q_9 have been evaluated as a function of q_7 according to the first postural synergy [24]. Simulation results are shown in Figure 4a.

The second simulation refers to tendon configuration in Figure 2b, in which the index is actuated with two tendons connected together in the proximal part and then actuated with the same motor. Moreover, in this case, the simulated movement is finger flexion starting from the reference configuration, in this

Table VIII. *Index actuation with two tendons, flexion, and extension. Anchor points coordinates in the local reference frames.*

Tendon id.	Anchor id.	$x_a^{f,l}$ (mm)	$y_a^{f,l}$ (mm)	$z_a^{f,l}$ (mm)	Note on anchor point position
1					
	$A_{1,2,4,1}$	19	0	0	Finger tip
	$A_{1,2,4,2}$	0	−5	0	Along DIP axis
	$A_{1,2,3,3}$	12	−7	0	Middle of IP
	$A_{1,2,2,4}$	17	−8	0	Middle of PP
	$A_{1,0,0,5}$	52	−8	−20	Palm
	$A_{1,0,0,7}$	29	−8	−20	Palm
	$A_{1,0,0,8}$	0	−7	−15	Wrist
	$A_{1,-1,0,9}$	−23	−10	−10	Forearm
2					
	$A_{2,2,4,1}$	19	0	0	Finger tip
	$A_{2,2,4,2}$	0	5	0	Along DIP axis
	$A_{2,2,3,3}$	12	5	0	Middle of IP
	$A_{2,2,2,4}$	17	5	0	Middle of PP
	$A_{2,0,0,5}$	52	7	−20	Palm
	$A_{2,0,0,6}$	29	7	−20	Palm
	$A_{2,0,0,7}$	0	7	−15	Wrist
	$A_{2,-1,0,8}$	−23	−10	−10	Forearm

Table IX. *Wrist actuation with five tendons, flexion/extension, radial/ulnar deviation, pronation/supination. Anchor points coordinates in the local reference frames.*

Tendon id.	Anchor id.	$x_a^{f,l}$ (mm)	$y_a^{f,l}$ (mm)	$z_a^{f,l}$ (mm)	Note on anchor point position
1					
	$A_{1,1,1,1}$	0	0	0	Thumb MCP joint
	$A_{1,-1,0,2}$	−23	−10	−10	Forearm, bottom part
2					
	$A_{2,0,0,1}$	32	−10	12	Palm
	$A_{2,-1,0,2}$	−23	−10	−10	Forearm, bottom part
3					
	$A_{3,0,0,1}$	32	10	0	Hand back
	$A_{3,-1,0,2}$	−23	10	−10	Forearm, upper part
4					
	$A_{4,0,0,1}$	5	0	22	Lateral part of the palm
	$A_{4,-1,0,2}$	−15	0	−31	Forearm, lateral part
	$A_{4,-1,0,3}$	−23	10	−10	Forearm, upper part
5					
	$A_{5,0,0,1}$	5	0	−22	Lateral part of the palm
	$A_{5,-1,0,2}$	−15	0	31	Forearm, lateral part
	$A_{5,-1,0,3}$	−23	10	10	Forearm, upper part

case, it is not possible to actuate the MPC adduction/abduction movement, that would require different tendon strokes. The final value for q_7 joint has been set also in this case to 60°, while q_8 and q_9 have been evaluated as a function of q_7 according to the first postural synergy. Simulation results are shown in Figure 4b.

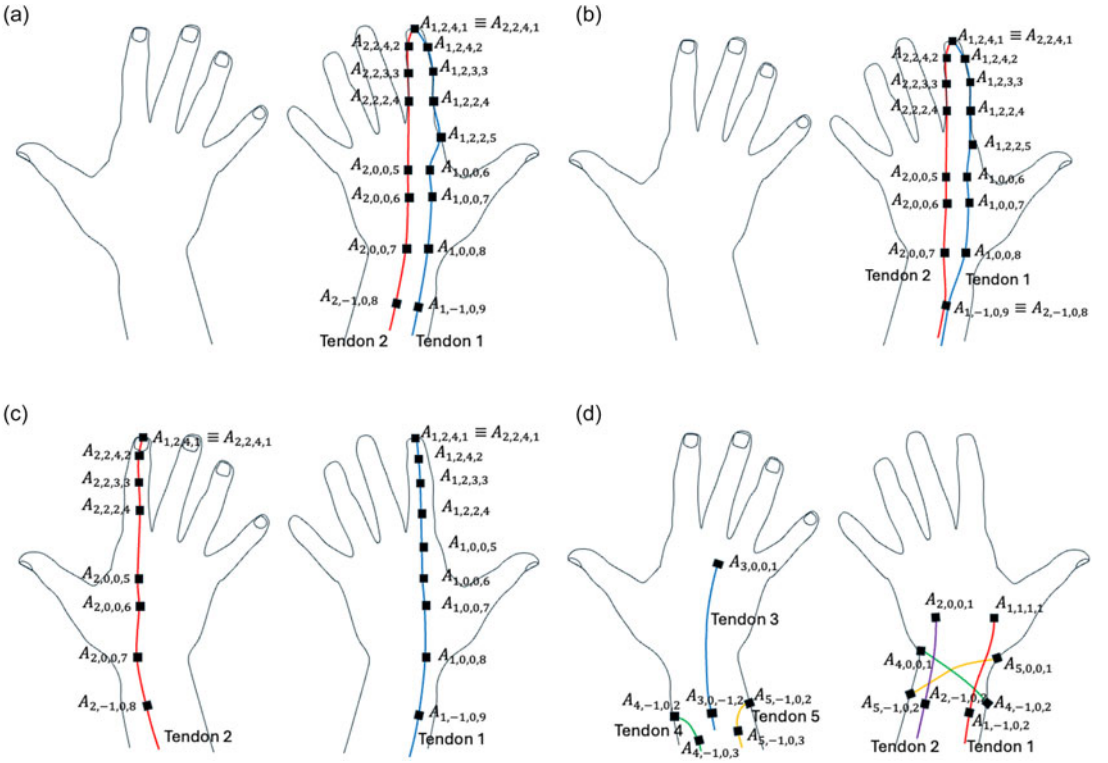

Figure 3. *Four examples of tendon arrangements a) finger actuation with two tendons, adduction/abduction, and flexion. b) Index actuation with two tendons connected to the same TSA, flexion. c) Index actuation with two tendons, flexion and extension. d) Wrist actuation with five tendons, flexion/extension, radial/ulnar deviation, and pronation/supination.*

Since in these two configurations, tendons are close to the hand coronal plane in the reference configuration, finger movement can be obtained with limited tendon strokes (lower than 10 *mm*). This relevant transmission ratio has an impact on force transmission, i.e., high tendon forces are needed to resist hand resistance. This configuration is then convenient when the patient using the device has low residual force and low spasticity.

The third and fourth simulations refer to tendon configuration in Figure 2c, in which the index is actuated with two independent tendons, approximately on the finger sagittal plane, actuating finger flexion and extension. For finger flexion, the same joint values used in the previous simulations have been employed, while in the extension the finger started from such flexed configuration and returned to the reference position. Simulation results are shown in Figure 4c and d.

In this case, since the tendon has a larger distance from the coronal plane, the transmission ratio is higher, in other terms, higher tendon strokes are needed to flex (and extend) the finger with respect to the previous cases (up to 35 *mm*). From the design point of view, this solution needs longer twisting zones. On the other hand, the higher transmission ratio is more suitable to apply high forces. The results of these numerical simulations are useful to evaluate the needed tendon pre-twist. It is worth to note that TSAs and tendons can only apply forces in one direction, i.e., they can only properly work when they are tight. However, during each exercise, some tendons need to be pulled while others are released. To allow for this, suitable pre-twist values must be applied to the tendons. For instance, during finger flexion (Figure 4c), tendon 1 is pulled while tendons 2 is released. Proper pre-stretch values, achieved by applying pre-twists to the TSAs, ensure that the exercises are executed smoothly and correctly.

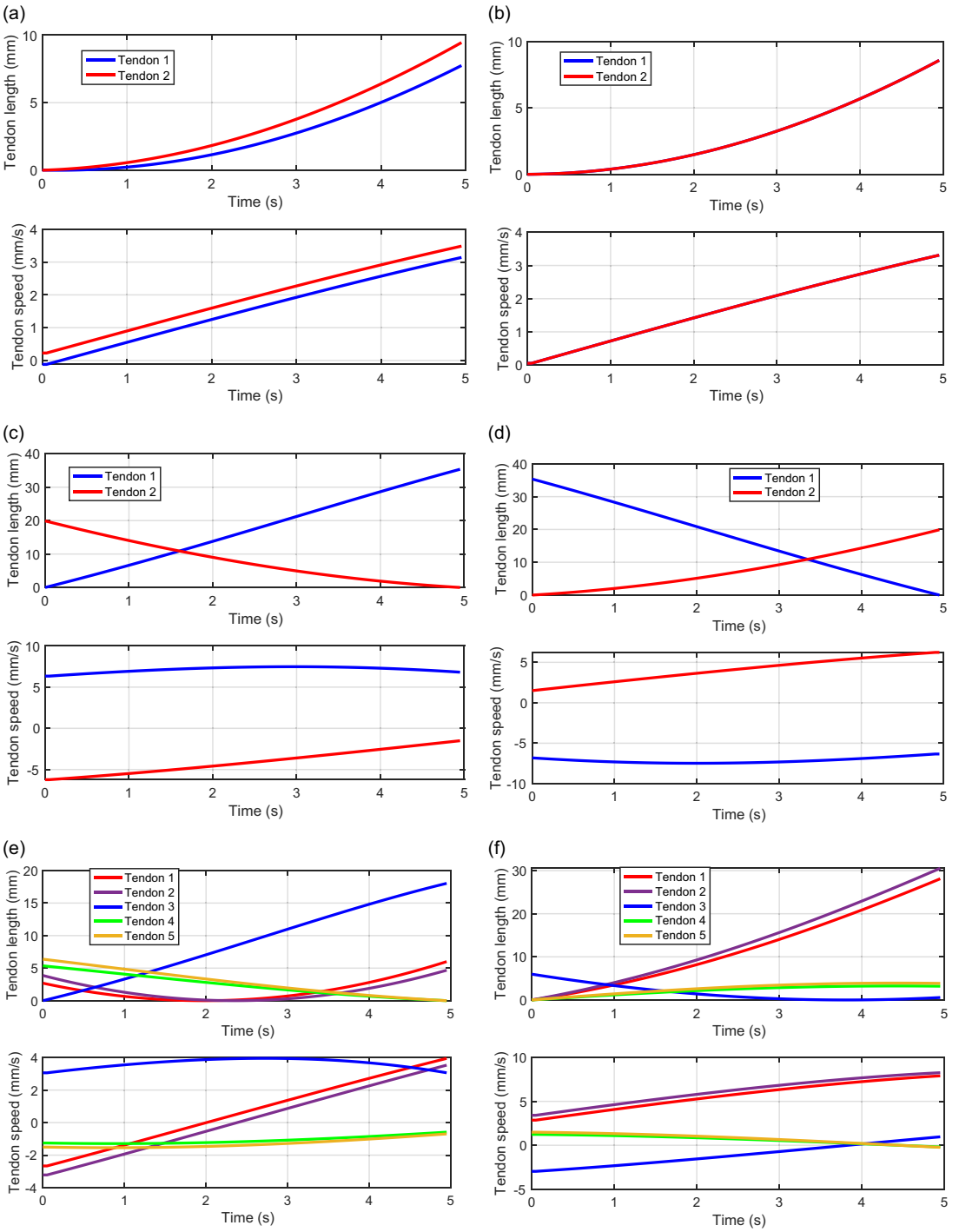

Figure 4. *Results of kinematic simulations: tendon length variations and tendon speeds. a) Index finger flexion obtained with tendon configuration in Figure 2a or Figure 2b. b) Index finger flexion and adduction, obtained with tendon configuration in Figure 2a. c) Index finger flexion obtained with tendon configuration in Figure 2c. d) Index finger extension obtained with tendon configuration in Figure 2c. e) Wrist extension obtained with tendon configuration in Figure 2d. f) Wrist flexion obtained with tendon configuration in Figure 2d.*

To show how the proposed system can be adapted to realize complex movements, the fifth and sixth simulations refer to a complete three-dimensional wrist motion, realized with five tendons arranged as shown in Figure 2d. The first three tendons are routed along the neutral axis, i.e., the axis formed by the hand and the forearm when aligned. Actuating tendon 3 and releasing tension from tendons 1 and 2, extends the wrist, while synchronously activating tendons 1 and 2 and releasing tendon 3 flexes the wrist. When actuating asynchronously the tendons 1 and 2, attached to hand palm, while keeping fixed tendon 3, the abduction/adduction movements are obtained. Simulation results in Figure 4e and 4f are relative to a flexion/extension exercise, with q_{26} ranging from 0 to 90° in the extension and from 0 to −90° in the flexion.

4. Actuated glove prototypes

Prototypes of the glove, actuating the thumb and the index finger, have been realized. The device mainly consists of three parts: a flexible glove, the actuation unit, and the electronic unit. Figure 1 shows two glove prototypes worn by two users, in which the thumb and the index are actuated with two tendons each. We designed the glove following the principles of user-centered device development. It is composed of a flexible part that completely envelops the hand, a modular compliant structure for each finger, and the actuators/control units. The compliant structure for the fingers supports the tendons in obtaining the right finger movement during the flexion and passively supports the extension. It can be connected to the main glove part in correspondence with the MCP joint in adjustable positions. Adjustable bands secure the compliant structure to the finger phalanges, ensuring user comfort and precise movement control. These bands play a pivotal role as they guarantee the correct routing of the tendons along the coronal plane of each finger through the embedded anchor points. Compared to the version presented in ref. [15], this version has significant ergonomic improvements. The glove can easily adapt to various hand sizes thanks to the multiple adjustment points. A novel, versatile flexible band has been realized to accommodate the actuation unit in different positions along the bracelet. This innovative design facilitates the generation of pulling forces within the glove, powered by the TSAs, (two TSAs for each finger). These actuators enable the precise execution of adduction/abduction, and flexion movements for both the thumb and index fingers. Each single actuation unit module is composed of the TSA and its support. The TSA is composed of a DC motor, Micro metal gear with 30:1 transmission ratio equipped with magnetic encoders that rely on a magnetic disc and Hall effect, and two tendons (polyethylene Dyneema fiber, Japan). To ensure the connection between tendons and the motor shaft, an embedded ball bearing within the module, minimizes friction during tendon twisting movements. Additionally, a pin has been integrated into the module to facilitate the separation between the twisting and the straight part. The length of each module has been defined to ensure optimal functionality and user comfort. The straight part of the tendon comes out of the actuation module and is routed through the anchor points on the palm and in the lateral parts of each compliant finger structure, according to the scheme previously introduced and reported in Figure 2a. The tendon is finally fixed to the index fingertip through locking pins, to prevent the tendons from detaching. The glove is manufactured using fused deposition modeling (FDM) 3D-printing technique, with polylactic acid (PLA) material for the rigid parts and Flex-45 thermoplastic co-polyurethane for soft parts, the device position-based control is performed by a Teensy 3.2 microcontroller.

Figure 5 shows CAD models of the different system components, specifically the glove, the finger module, and the band worn on the forearm, hosting the TSA motors and the twisting zone. Figure 6 shows the integration of the modules for index finger actuation, with an innovative structure similar to the one presented in Figure 2a, employing two motors and two gear systems and enabling flexion/extension and adduction/abduction with two motors only. Two pairs of independent tendons are employed (highlighted in yellow and green, respectively). Green tendons actuate finger extension, and yellow tendons actuate finger flexion. When the motors rotate synchronously, adduction/abduction is actuated, when they rotate asynchronously, flexion/extension is actuated.

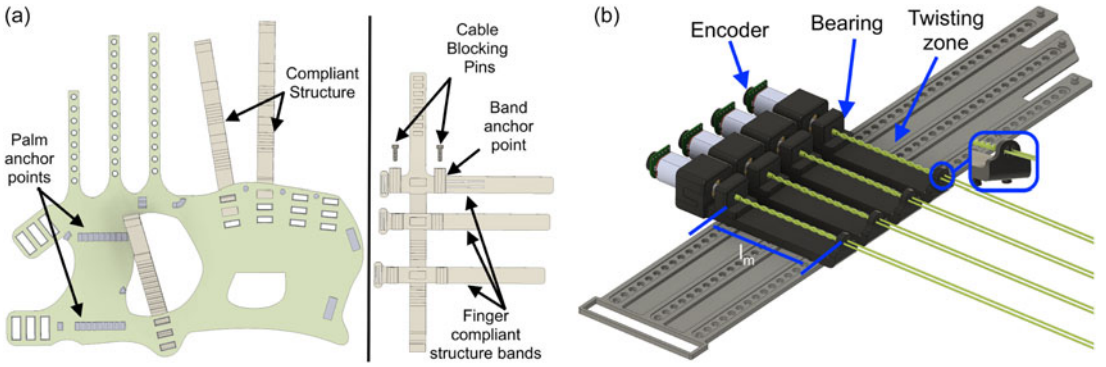

Figure 5. *a) Wearable glove (left) and finger module (right) CAD models, the finger module is composed of a passive element for controlling finger extension motion and three rings for the connection to the finger and tendon routing. b) Forearm bracelet CAD model. TSAs are connected to a flexible and adaptable band worn close to the wrist.*

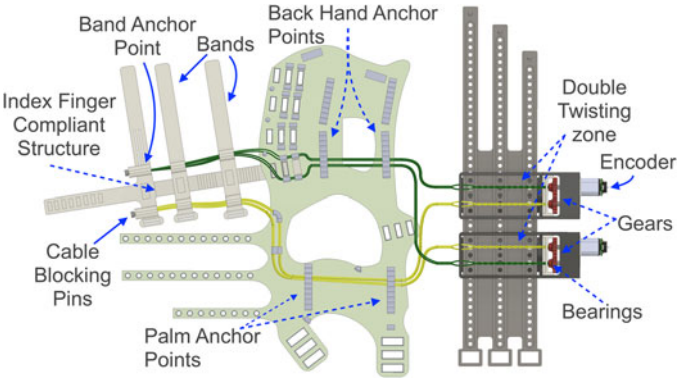

Figure 6. *Glove CAD model for fingers flexion/extension, abduction/adduction. The left part of the model includes the glove, while the right part includes the band with the actuation, which is composed of two TSAs, including a gear system, working in a coupled way. Tendons highlighted in green actuate finger extension, the ones highlighted in yellow actuate flexion. Rotating the motors synchronously, adduction/abduction is actuated, an asynchronous actuation produces flexion/extension motion.*

5. Preliminary experiment results

We realized and tested two prototypes of the index finger actuation. The first exploits two TSAs to implement flexion/extension and adduction/abduction while the second uses a single TSA to implement flexion-extension of the finger (Figure 2). In the first case, for each of the two actuation modules, the four outgoing tendons are routed and anchored through the locking pins to the fingertip of the index finger, as schematized in Figure 2a. In the second case, only one TSA is used and the two tendons from the actuation module are routed as in Figure 2b.

The tests were performed by a user with reduced hand mobility, low force, and no spasticity. Since the glove is tailored to the user's specific characteristics and needs, the testing and evaluation phase involved a single participant, following the "single-case design" methodology. This approach, used in clinical research, involves analyzing data from one individual and can yield robust experimental evidence [25]. The experimental protocols complied with the Declaration of Helsinki, and there was no risk of harm to the participant's health. Data collection followed the European General Data Protection Regulation (GDPR) 2016/679, with all data stored locally and used solely for post-processing analysis. No sensitive personal information was recorded.

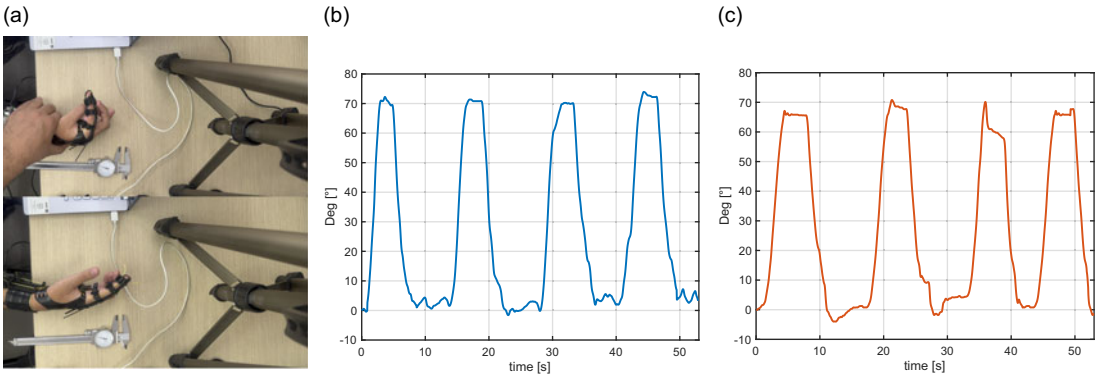

Figure 7. *Tests with the actuated glove. a) A user performing a flexion exercise with the index glove. b,c) Results of a representative flexion/extension trial in case of b) with two modules (Figure 2a) and c) one module (Figure 2b). Both the diagrams report MPC flexion angle as a function of time.*

Three types of tests were carried out: flexion/extension with the configuration reported in Figure 2b and flexion/extension, abduction/adduction using the configuration of Figure 2a. All tests were repeated five times with the user's hand fixed on the table in the same position. Each test consisted of repeating the flexion movement four times within a 60 s. The exercises were recorded and the videos were elaborated using the software Kinovea. Based on the results of the simulations presented in the previous section and on TSA characterization discussed in ref. [15], we realized the actuation support with the twisting part length equal to $l_m = 53\,mm$, which allows a maximum MPC flexion of approximately 80°. The results obtained in the case of flexion motion with the Figure 2a routing system, are 71.49° ± 2.19° while for adduction/abduction is 30.46° ± 0.57°. With regard to the results obtained with the Figure 2b configuration in terms of maximum MCP index angle it is 69.43° ±2.08°. In Figure 7, the profiles of two sample trials, one for each type of test, are reported and in Table X, and the main results are summarized.

6. Discussion

The preliminary tests involving a potential user presented in the previous section demonstrated its potential outcomes (the O term in the PICO framework) in terms of hand joint ROM recovery. To assess and monitor system outcomes, the device needs to be equipped with sensors to detect the user's hand movements and force and provide their feedback.

The prototypes and the tests described in the previous section were aimed at preliminary verification that the proposed actuated glove can be effective in the actuation of hand motion. The user reported that the system was easy to wear with little assistance, light, and comfortable. The results of the preliminary trials showed that the active movement obtained was compatible with the user's finger ROM. The user did not report any discomfort, disturbances, or pain while performing the exercise.

It should be noted that the underactuated, flexible, and adaptable structure of the glove needs an initial calibration phase at the beginning of the exercise and training session, necessary to ensure that all tendons are properly tight. This procedure has been performed manually in the experiments described above. An automatic calibration procedure is needed and will be implemented in future developments of the system.

The compliant and underactuated structure further requires proper tracking systems. In the preliminary evaluation presented, system tracking was needed only for evaluation purposes; so, it was performed by post-processing and elaborating video-recorded exercises. The movement amplitude and frequency were manually set, and no direct feedback control was implemented. To make the device available to users, a specific tracking system is needed. In devices previously developed [4], we employed a tracking system based on inertial measurement units (IMU). This system will be implemented on the future

Table X. *Comparison of performance metrics between Two-TSA and Single-TSA configurations.*

	Two-TSA Config	**Single-TSA Config**
Maximum MCP Flexion Angle from Figure 7b,c (°)	71.49 ± 2.19	69.43 ± 2.08
Repeatability of MCP Flexion Angle among all four tests (°)	8.31	6.89
Repeatability of MCP Abduction/Adduction Angle among all four tests (°)	8.00	N/A
Actuation speed ($^\circ/s$)	20.06 ± 0.81	17.78 ± 1.59
Estimated maximum output force (N) [15]	17.95 ± 1.04	9.02 ± 1.22

developments of the TSA-actuated glove presented in this work. More specifically, the tracking system implemented for the wrist module described in ref. [26] will be extended to hand tracking.

Specific position and impedance control systems, together with an accessible graphical user interface for exercise selection and monitoring, are also needed to make the glove available to the user for autonomous use of the system in rehabilitation contexts.

According to the design flowchart presented in ref. [3], after completing the design with the sensing, control, and user interface, an extensive testing phase is needed. This phase consists of two parts: *functional testing* and *clinical testing*. The first one includes tests on multiple healthy subjects, motion testing, exercise testing, safety functions testing, and device functional evaluation. The second includes tests in patients with hand motor dysfunction and a clinical evaluation of the device.

In ref. [3], wearable exoskeletons for the hand were classified in *rigid* (with rigid, link-based transmission mechanisms), *soft* (exoskeletons formed by easily deformable materials and textile materials), and *hybrid*. The device proposed in this paper falls within *soft* type. Considering the requirements introduced in Section 1, a soft ecoskeleton was considered more convenient with respect to rigid or hybrid ones, since it presents remarkable adaptability and flexibility properties, while the level of forces and precision required is not very high. A comparative analysis of TSA-based actuated gloves with other robotic gloves for hand rehabilitation and assistance that have emerged over the past decade in terms of actuation, transmission, mechanical structure, number of fingers actuated, tip force, system weight, portability, type of motion, modularity, and intrinsic safety is presented in ref. [15].

7. Conclusion

In this work, we present analysis of a TSA-based modular actuated glove for hand rehabilitation. We focused on the realization of a mathematical model enabling the evaluation of glove kinematic performance based on tendon anchor point arrangement. The hand model is 28 DOF and parametric, so it can be adapted to different hand sizes by adjusting only two parameters, namely the length and width of the hand. In addition to the hand model, glove actuation is parametrized by defining anchor point positions and tendons' routing in a systematic way and by providing inverse and differential kinematic relationships. The model is applied to the analysis of four specific glove configurations; however, its general structure allows easy adaptation to test and compare different actuation solutions. We exploited different solutions for finger actuation, and we realized prototypes for two of them: in the first, two pairs of independent TSAs actuate the finger flexion/extension and adduction/abduction movements, and in the second, a pair of tendons connected to a single TSA actuate the finger flexion movement. As shown in the analysis, the proposed system is modular and extensible to various types of hand and finger actuation.

Future developments will exploit the proposed methodology using both numerical simulations and experimental activities. Concerning hand model, it will be further detailed with parameters for dynamic behavior representation. Hand muscle actuation will be introduced to simulate resistance during rehabilitation exercises and to simulate specific pathologies. We will focus on further analyzing the

role of tendons' anchor points' positions and routing paths on system performance. Optimization procedures will be implemented to define the most convenient glove configuration according to system requirements. The model will be adapted to simulate the interaction with other types of exoskeleton, including rigid and hybrid types. Future developments of the model will also consider more realistic conditions, as the friction in anchor point constraints, the friction due to tendon sliding over glove surface, tendon elasticity, and TSA actuation properties.

The design of the device proposed in this paper was focused on rehabilitation applications. However, its flexible and adaptable structure, the versatility of the actuation system, and the ease of wearing and use make the device suitable for assistive applications, too. For this application, however, further developments are needed to provide the device with a proper sensing system and a force control system, needed to an effective and safe human-robot interaction.

Author contributions. MD and MM conceived and designed the study. MM realized the mathematical model and performed numerical analyses. MD and AP realized the prototypes and conducted experimental data gathering. MD, AP, and MM wrote the article.

Financial support. This work was supported by the European Union by the Next Generation EU project ECS00000017 'Ecosistema dell'Innovazione' THE - Tuscany Health Ecosystem (Spoke 9: Robotics and Automation for Health) and the project "SAILOR: Soft wearable robotic glove for hand theranostics" funded by the MIUR Progetti di Ricerca di Rilevante Interesse Nazionale (PRIN) Bando 2022 – grant 20229PYMRA.

Competing interests. The authors declare no conflicts of interest exist.

Ethical standards. The authors assert that all procedures contributing to this work comply with the ethical standards of the relevant national and institutional committees on human experimentation and with the Helsinki Declaration of 1975, as revised in 2008.

References

[1] A. B. Payedimarri, M. Ratti, R. Rescinito, K. Vanhaecht and M. Panella, "Effectiveness of platform-based robot-assisted rehabilitation for musculoskeletal or neurologic injuries: A systematic review," *Bioengineering* **9**(4), 129 (2022).
[2] B. Östlund, M. Malvezzi, S. Frennert, M. Funk, J. Gonzalez-Vargas, K. Baur, D. Alimisis, F. Thorsteinsson, A. Alonso-Cepeda, G. Fau, F. Haufe, M. Di Pardo and J. C. Moreno, "Interactive robots for health in europe: Technology readiness and adoption potential," *Front. Publ. Health* **11**, 979225 (2023).
[3] G. M. Achilli, C. Amici, M. Dragusanu, M. Gobbo, S. Logozzo, M. Malvezzi, M. Tiboni and M. C. Valigi, "Soft, rigid, and hybrid robotic exoskeletons for hand rehabilitation: Roadmap with impairment-oriented rationale for devices design and selection," *Appl. Sci.* **13**(20), 11287 (2023).
[4] M. Dragusanu, M. Z. Iqbal, T. L. Baldi, D. Prattichizzo and M. Malvezzi, "Design, development, and control of a hand/wrist exoskeleton for rehabilitation and training," *IEEE Trans. Robot.* **38**(3), 1472–1488 (2022).
[5] M. Dragusanu, D. Troisi, A. Villani, D. Prattichizzo and M. Malvezzi, "Design and prototyping of an underactuated hand exoskeleton with fingers coupled by a gear-based differential," *Front. Robot. AI* **9**, 862340 (2022).
[6] N. Banović, F. Marić, M. Seder and I. Petrović, "Kinematic modelling and design of a tendon actuated soft manipulator," *IFAC-PapersOnLine* **55**(38), 13–18 (2022).
[7] M. Tiboni and C. Amici, "Soft gloves: A review on recent developments in actuation, sensing, control and applications," *Actuators* **11**, 232 (2022).
[8] M. Hosseini, R. Meattini, G. Palli and C. Melchiorri, "A wearable robotic device based on twisted string actuation for rehabilitation and assistive applications," *J. Robot.* **2017**, 1–11 (2017).
[9] D. Popov, I. Gaponov and J. H. Ryu, "Bidirectional Elbow Exoskeleton Based on Twisted-string Actuators." **In:** 2013 IEEE/RSJ International Conference on Intelligent Robots and Systems, IEEE (2013) pp. 5853–5858.
[10] R. Müller, M. Hessinger, H. Schlaak and P. Pott, "Modelling and characterisation of twisted string actuation for usage in active knee orthoses," *IFAC-PapersOnLine* **48**(20), 207–212 (2015).
[11] H. S. Seong, D. H. Kim, I. Gaponov and J. H. Ryu, "Development of a Twisted String Actuator-based Exoskeleton for Hip Joint Assistance in Lifting Tasks." **In:** 2020 IEEE International Conference on Robotics and Automation (ICRA), IEEE (2020) pp. 761–767.
[12] M. Hosseini, A. Sengül, Y. Pane, J. De Schutter and H. Bruyninck, "Exoten-glove: A Force-Feedback Haptic Glove Based on Twisted String Actuation System." **In:** 2018 27th IEEE International Symposium on Robot and Human Interactive Communication (RO-MAN) (IEEE, 2018) pp. 320–327.

[13] G. Palli, C. Natale, C. May, C. Melchiorri and T. Wurtz, "Modeling and control of the twisted string actuation system," *IEEE/ASME Trans. Mechatron.* **18**(2), 664–673 (2012).
[14] D. Bombara, S. Fowzer and J. Zhang, "Compliant, large-strain, and self-sensing twisted string actuators," *Soft Robot.* **9**(1), 72–88 (2022).
[15] M. Dragusanu, D. Troisi, B. Suthar, I. Hussain, D. Prattichizzo and M. Malvezzi, "MGlove-TS: A modular soft glove based on twisted string actuators and flexible structures," *Mechatronics* **98**, 103141 (2024).
[16] C. Amici, R. Buraschi, M. Dragusanu, M. Gobbo, S. Logozzo, M. Malvezzi, J. Pollet, M. Tiboni and M. C. Valigi, "Beyond Boundaries: Pico-Driven Design Criteria for Robotic Rehabilitation Medical Devices," **In:** *International Workshop IFToMM for Sustainable Development Goals* (Springer, 2025) pp. 285–292.
[17] P. Beckerle, G. Salvietti, R. Unal, D. Prattichizzo, S. Rossi, C. Castellini, S. Hirche, S. Endo, H. B. Amor, M. Ciocarlie, F. Mastrogiovanni, B. D. Argall and M. Bianchi, "A human–robot interaction perspective on assistive and rehabilitation robotics," *Front. Neurorobot.* **11**, 24 (2017).
[18] M. Malvezzi, G. Gioioso, G. Salvietti and D. Prattichizzo, "Syngrasp: A matlab toolbox for underactuated and compliant hands," *IEEE Robot. Autom. Mag.* **22**(4), 52–68 (2015).
[19] M. Pozzi, G. M. Achilli, M. C. Valigi and M. Malvezzi, "Modeling and simulation of robotic grasping in simulink through simscape multibody," *Front. Robot. AI* **9**, 873558 (2022).
[20] E. Peña-Pitarch, N. T. Falguera and J. Yang, "Virtual human hand: Model and kinematics," *Comput. Method Biomech. Biomed. Eng.* **17**(5), 568–579 (2014).
[21] I. M. Bullock, J. Borràs and A. M. Dollar, "Assessing Assumptions in Kinematic Hand Models: A Review." **In:** 2012 4th IEEE RAS & EMBS International Conference on Biomedical Robotics and Biomechatronics (BioRob) (IEEE, 2012) pp. 139–146.
[22] B. Siciliano and O. Khatib. "Robotics and the Handbook." **In:** *Springer Handbook of Robotics* (Springer, 2016) pp. 1–6.
[23] I. Gaponov, D. Popov and J.-H. Ryu, "Twisted string actuation systems: A study of the mathematical model and a comparison of twisted strings," *IEEE/ASME Trans. Mechatron.* **19**(4), 1331–1342 (2013).
[24] M. Gabiccini, A. Bicchi, D. Prattichizzo and M. Malvezzi, "On the role of hand synergies in the optimal choice of grasping forces," *Autonomous Robots* **31**, 235–252 (2011).
[25] T. R. Kratochwill, J. Hitchcock, R. H. Horner, J. R. Levin, S. L. Odom, D. M. Rindskopf and W. R. Shadish, "Single-case designs technical documentation," *What works clearinghouse* (2010). https://scholar.google.com/scholar?hl=it&as_sdt=0%2C5&q=Single-case+designs+technical+documentation.+What+works+clearinghouse&btnG=#:~:text=includi%20citazioni-,%5BPDF%5D%20ed.gov,-Single%2Dcase%20designs.
[26] M. Dragusanu, N. Guinet, B. Suthar, T. L. Baldi, D. Prattichizzo and M. Malvezzi, "A 3 degrees-of-freedom lightweight flexible twisted string actuators (tsas)-based exoskeleton for wrist rehabilitation," *IEEE Robot. Autom. Lett.* **10**, 6520–6527 (2025).

Cite this article: M. Dragusanu, A. Piroli and M. Malvezzi, "Analysis and development of the modular elements of a tendon-actuated glove for hand rehabilitation", Robotica. https://doi.org/10.1017/S0263574725102464